AIAA JOURNAL
Vol. 32, No. 6, June 1994

Aerodynamic Investigation with Focusing Schlieren in a Cryogenic Wind Tunnel

Ehud Gartenberg*
Old Dominion University, Norfolk, Virginia 23529
and
Leonard M. Weinstein† and Edwin E. Lee Jr.‡
NASA Langley Research Center, Hampton, Virginia 23681

A flow visualization study was performed using a focusing schlieren system in the 0.3 m Transonic Cryogenic Tunnel at NASA Langley Research Center. The system proved to be a useful flow visualization tool for flows as low as $M = 0.4$. This study marked the first verification of the focusing schlieren technique in a major subsonic/transonic wind tunnel and the first time that high-quality, detailed pictures of high-Reynolds-number flows were obtained in a cryogenic wind tunnel. This test was part of a development program to implement instrumentation techniques in cryogenic wind tunnels, with the ultimate aim to use them in the National Transonic Facility.

Nomenclature

A = clear aperture (diameter) of focusing schlieren lens
a = light source image height above cutoff
b = width of cutoff opaque strip
DS = depth of sharp focus
DU = depth of unsharp focus
d = opening of rudder aerobrake
F = focal length of focusing schlieren lens
f = "f number" of focusing schlieren lens, F/A
k = number of line pairs of lens resolution per mm
L = distance from source grid to focusing schlieren lens
L' = distance from focusing schlieren lens to cutoff grid location
l = distance from object flowfield plane to focusing schlieren lens
l' = distance from focusing schlieren lens to image location
M = Mach number
m = magnification ratio, l'/l, L'/L, etc.
n = grid lines per unit length at cutoff
p = pressure
R = Reynolds number
S = Strouhal number
T = temperature
w = diffraction limited resolution of focusing schlieren in the focused plane of the flow
α = angle of attack
ε_{min} = refractive angle change causing 10% brightness change in image for focusing schlieren
λ = vortex wavelength
ϕ = number of blended pair lines in focusing schlieren image

Subscripts
L = value based on model length
t = stagnation condition
∞ = freestream condition

Received July 31, 1993; presented as Paper 93-3485 at the AIAA 11th Applied Aerodynamics Conference, Monterey, CA, Aug. 9–11, 1993; revision received Nov. 23, 1993; accepted for publication Nov. 30, 1993.

*Research Associate Professor, Department of Mechanical Engineering and Mechanics. Senior Member AIAA.
†Aerospace Technologist, Experimental Flow Physics Branch, MS 170. Associate Fellow AIAA.
‡Aerospace Technologist, High-Reynolds-Number Aerodynamics Branch, MS 267. Senior Member AIAA.

Introduction

THE design and flight testing of large transport airplanes in the mid-sixties indicated the critical need for wind-tunnel testing capability to match not only the flight Mach number but also the Reynolds number as well.[1,2] This conclusion was reached after some prototypes displayed aerodynamic characteristics different from their design values, and the mismatch was traced to "Reynolds number effects." This term refers to changes in flow behavior induced by viscous and boundary-layer effects that are attributed to the substantially higher Reynolds number of an airplane in flight compared with its model in wind-tunnel testing. To solve this problem, cryogenic wind tunnels with nitrogen gas as the working fluid have been built,[3] where flight Reynolds numbers are produced by combining low temperatures (as low as 100 K) and moderate pressures (up to 10 ata). NASA Langley operates the largest and most capable wind tunnel of this kind in the world, the National Transonic Facility (NTF), with a test section of 2.5×2.5 m, and a Reynolds number capability of up to 460×10^6 per meter at Mach 0.85. NASA Langley also operates the 0.3 m Transonic Cryogenic Tunnel (0.3 m TCT) with a test section of 0.3×0.3 m and adaptive walls. This tunnel is used mainly for two-dimensional airfoil testing and for development of experimental techniques. Worldwide, there are approximately 16 other facilities serving various purposes, from development of cryogenic wind-tunnel technology and test techniques to industrial testing at flight Mach and Reynolds numbers.

The work described herein is part of a research and development program to implement flow diagnostic techniques in cryogenic tunnels. Some of the more necessary techniques (e.g., flow visualization and boundary-layer transition detection) could not be previously implemented directly in cryogenic tunnels, and it was only during the last three years that progress was made in this direction. Among these techniques, flow visualization is considered a critical element for studies of high-Reynolds-number flows, Reynolds-number effects, and monitoring of buffet onset.

Focusing Schlieren Design

An early evaluation of possible flow visualization techniques identified focusing schlieren as the most promising candidate for the following reasons: large field of view, focusing capability, high sensitivity, robustness to optical interference, and low cost.

The flow image obtained by sharply focusing on a plane inside the test section contributes directly to the technique's robustness to optical interference. This feature allows use of low-grade windows and other optical components, which bears directly on the low cost. In addition, in those transonic tunnels where the system has to be placed outside the tunnel, the large turbulent structures in the

plenum are blurred out of focus, thus permitting the use of this technique where regular schlieren systems often fail.

The low cost of the optical components used in focusing schlieren systems is important on its own, and it also bears on the technique's operational flexibility and range of application. For example, it makes it possible to tailor a system for particular requirements, while retaining for common use the more expensive components such as the illumination source, the image acquisition devices, and possibly the focusing lens. This stands in sharp contrast with conventional schlieren systems, where the high cost of the optical components may deter, or prohibit altogether, adapting an existing system to different requirements.

A minor disadvantage of this technique is the dependence of the image magnification ratio on the location of the focused plane across the wind-tunnel test section. However, actual dimensions of flow structures can be deduced by direct comparison with the model size.

The analysis and practice of focusing schlieren is detailed in Ref. 4. This paper reviews only those aspects that are considered essential for the understanding of this design and that shed light on particular aspects of cryogenic-tunnel application.

The starting point is some practical guidelines for focusing schlieren preliminary design and performance analysis. Assuming a satisfactory lens was selected (in terms of focal length F, field of view, and resolution), an initial step may be to determine a value for a, the light source image height above cutoff. This parameter is used later to determine the width of the cutoff grid opaque strips. According to the flow regime of interest, we set an initial value for the sensitivity of the system ε_{min}, usually taken between 4 to 16 arcsec, and use Eq. (1) to determine a:

$$\varepsilon_{min}\,(\text{arcsec}) = \frac{20{,}626aL}{L'(L-l)} \tag{1}$$

or, using the thin lens formula,

$$\varepsilon_{min} = 20{,}626\frac{a}{F}\left[\frac{1-(F/L)}{1-(l/L)}\right] \tag{2}$$

To facilitate the initial iteration, some reasonable and simplifying assumptions can be made regarding the relationship between the various parameters, e.g., $L \geq$ test section width and $l \geq$ half the test section width. Therefore, $L = 2l$ is a good initial approximation for design iterations. By embedding these assumptions in Eq. (2), a value for a can be obtained. Before proceeding further, a should be checked against the resolution of the focusing lens to insure the desired performance of the system. Usually, lens resolution is given in terms of k number of line pairs (lp) per millimeter (the numerical value of k can vary between 15 lp/mm for poor lens to 60 lp/mm for high-quality lens, and the most commonly used lens are designed for 30 lp/mm). It must be verified that

$$a \geq 2/k \tag{3}$$

i.e., it takes at least 2 line pairs of lens resolution to sharply define a.

Next, the designer should set n. Equation (4) gives the number of pairs of blended lines ϕ in focusing schlieren image in terms of n and the clear aperture (diameter) A of focusing schlieren lens

$$\phi = \frac{An}{2}\left[1-\frac{1-(F/l)}{1-(F/L)}\right] \tag{4}$$

Solved for n, this equation yields the linear density of lines of the cutoff grid, provided ϕ is known. The experience gathered so far indicates that $\phi \geq 5$ works satisfactorily; however, at times this parameter may be constrained to slightly lower values that are still technically acceptable. With a first estimate of a and ϕ, the width b of the cutoff grid opaque strips may be calculated from

$$b = [(1/n)-2a] \tag{5}$$

thus completing the design of the cutoff grid. Since the magnification ratio is

$$m = L'/L \tag{6}$$

the opaque strips of the source grid should be b/m and the clear strips should be $2a/m$, which completes the design of the source grid. Once the source grid is made according to the dimensions just obtained, the cutoff grid is obtained by exposing in its place a photographic film to the source grid and developing the negative.

With the cutoff grid characteristics and the system's geometry known, the resolution w, the depth of sharp focus DS, and the depth of unsharp focus DU of the focusing schlieren system can be calculated as follows:

$$w = \frac{4l\lambda\phi}{Abn} \tag{7}$$

$$DS = 2\frac{l}{A}w \tag{8}$$

and

$$DU = 4\frac{l}{A} \tag{9}$$

in millimeters.

Focusing Schlieren System

A schematic layout of the focusing schlieren system for the 0.3 m TCT is shown in Fig. 1. Its various components were mounted on or inside the wind tunnel, causing the nominal distance between the illuminating and imaging optics to vary under the thermal effects of the structure. In the following discussion of the system's geometry, the original dimensions, that were calculated in inches, were converted to millimeters, usually rounded to the nearest integer figure. The distance from the source grid to the focusing (image) lens is L = 1575 mm (62 in.), the distance from the focusing lens to the cutoff grid is L' = 1003 mm (39.5 in.), the distance from the test section centerline (focused plane) to the focusing image lens is l = 1219 mm (48 in.), and the distance from the focusing lens to the relay Fresnel lens (image plane) is l' = 1219 mm (48 in.). The light source was a doubled frequency Nd:YAG laser, emitting green light at a wavelength of 0.52 μm. It was operated in an intermittent mode that fired energy pulses of 10–20 mJ for 10 ns at 30 Hz. The source Fresnel lens was made of two 419 × 419 mm^2 (16.5 × 16.5 in.^{2}) lenses, each having a 610 mm (24 in.) focal length, producing a combined focal length of 305 mm (12 in.). The source grid was made by nickel vapor deposition on Pyrex glass, with 6.5 lines/cm (16.4 lines/in.), with opaque strips b/m = 2 mm (0.08 in.) and clear strips of 0.5 mm (0.02 in.). The focusing lens was taken from a surplus aerial camera. It is a $f/6$ lens with a focal length of F = 610 mm (24 in.), a maximum clear aperture of A = 102 mm (4 in.), and a maximum resolution of 30 lp/mm. The original design of this system called for using the full aperture of 102 mm (4.0 in.); however, because

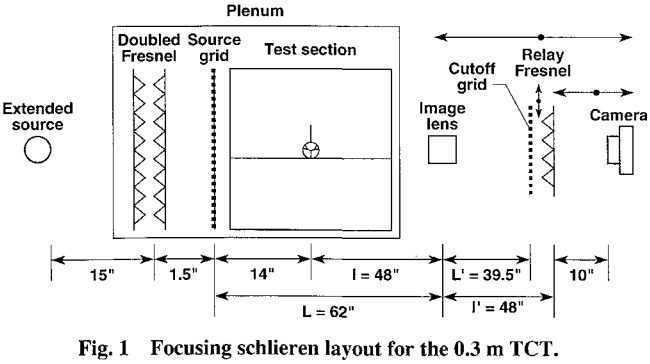

Fig. 1 Focusing schlieren layout for the 0.3 m TCT.

of inadequate sharpness of the image, it was decided to stop down the lens to a 69-mm (2.7-in.) aperture. However, this negatively affected the depth of the sharp and unsharp depth of focus [see Eqs. (8) and (9)] and the number of blended lines in the focusing schlieren image (because the grids remained the same [see Eq. (4)]. It should be noted that aerial camera lenses are designed for large object distances and lose performance at shorter object distances. This resulted in a loss of sharpness for the initial design.

Still pictures of the flow were taken with a 70-mm reflex photographic camera, using an ASA 400 film. This camera has a ground-glass viewer, which was imaged by a TV camera. The images were relayed to the control room for display and recording on a super-VHS videocassette recorder (S-VHS VCR). The magnification ratio of the image at the principal focus (relay Fresnel in Fig. 1) is $m = l'/l = 1$, but the relay Fresnel lens and the camera optics project the 275×275 mm image onto the 50×50 mm film at a reduction ratio of 5.5:1. The resolution of the film is about 50 lp/mm, and the super-VHS VCR format has about 400 columns by 256 lines per field.

The following details complete the specification of this system: light source image height above cutoff $a = 0.152$ mm (0.006 in.), cutoff opaque strip width $b = 1.245$ mm (0.049 in.), grid lines at cutoff $n = 6.5$ per cm (16.4 per in.), number of blended pair lines in focusing schlieren image $\phi = 3.9$, sensitivity $\varepsilon_{min} = 13.9$ arcsec, resolution in the focusing plane $w = 0.178$ mm (0.007 in.), depth of sharp focus $DS = 6$ mm (0.25 in.), and depth of unsharp focus $DU = 71$ mm (2.8 in.).

The receiving optics had three degrees of freedom, all of them adjustable from the control room. First, the mounting platform could be moved in and out of the tunnel window to compensate for the variable distance between the source grid and the cutoff grid caused by the thermal strains (expansion and contraction) of the tunnel. Second, the cutoff grid could be moved in a plane, perpendicular to the grid direction, to adjust the sensitivity or the brightness of the image. Third, the relay Fresnel lens and cameras could be moved together to change the imaged plane of the flow.

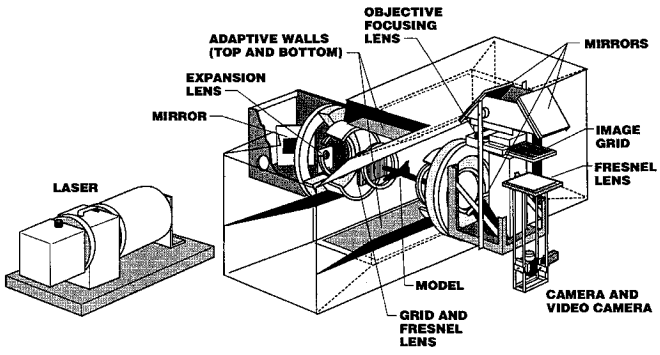

Fig. 2 Isometric view of the focusing schlieren mounting in the 0.3 m TCT.

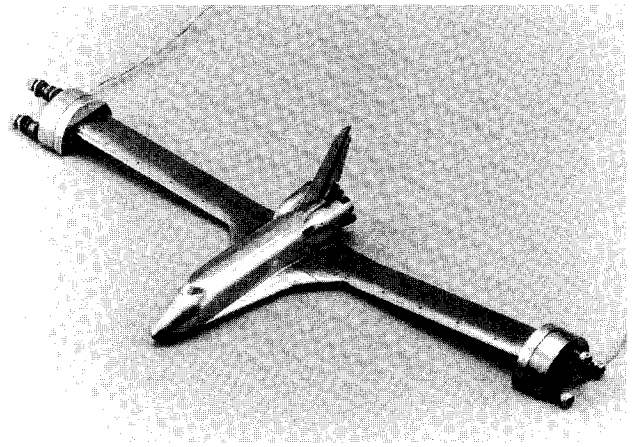

Fig. 3 Modified Space Shuttle model for the 0.3 m TCT: body length 150 mm, body length (including engine nozzles) 164 mm, span 330 mm, scale 0.0045.

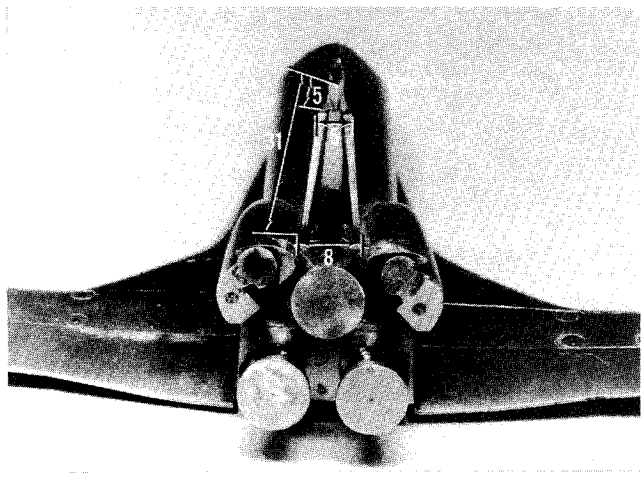

Fig. 4 Base of modified Space Shuttle model, dimensions in millimeters.

To maximize the system's field of view, the illuminating Fresnel lens and source grid had to be placed inside the wind-tunnel plenum, because the outside (plenum) windows of the tunnel were 203 mm (8 in.) in diameter, whereas the (polycarbonate) test section windows, between which the model was fixed, were 330 mm (13 in.) in diameter. No major damage was caused to any of these optical components, including the test section windows, resulting from their exposure to the extremely low temperatures. This is an encouraging outcome for the design of systems for large cryogenic tunnels, where the entire system may have to be placed inside the plenum.

An isometric view of the focusing schlieren system as it was actually installed in the tunnel is shown in Fig. 2. This figure also illustrates the extensive use of folding optics to keep the system as compact as possible. Notice the closed box attached to the tunnel wall that was continuously purged with dry gaseous nitrogen to keep moisture from forming on the tunnel window. Inside the box, the laser beam is turned 90 deg by a mirror, and then it is rapidly expanded by a fast lens into the plenum, illuminating the Fresnel lens and the source grid. Between the expanding lens and the tunnel window, there is also a diffuser (not shown in the figure), which makes the beam uniform. A good design will have the Fresnel lens project the image of the light source onto the clear area of the focusing lens, insuring that no light energy is dissipated on illuminating walls, and thus maximizing the brightness of the flow images.

The light-source energy pulse has to be short enough "to freeze" the motion of the flow structures on the recording medium. Also, the light energy delivered to the recording medium (i.e., film or sensor array) should match its sensitivity. For this particular case, the efficiency of the light pulse to freeze the flow can be estimated by assuming a $M_\infty = 0.85$ flow at $T_t = 320$ K. With a convective velocity ratio of 0.6, we get a convective velocity of 173 m/s, which is actually a conservative estimate for a cryogenic tunnel (where the flow temperatures are typically much lower, and so are the flow velocities at given Mach numbers). Nevertheless, even for such a high-limit case, a flow structure will travel 1.7 μm during the duration of one laser pulse, which is well under the distance imaged under the width of one line of the lens resolution (= 16 μm) or one line of the photographic-film resolution (= 55 μm).

Model

Figure 3 shows the model used in this experiment, which is reminiscent of a modified Space Shuttle. This model was used during the Space Shuttle design to study Reynolds number and model support effects on base drag. For this purpose, the model was supported by wingtips in the tunnel to free the base area from sting or strut interference, thus requiring extension of the wing tips out-

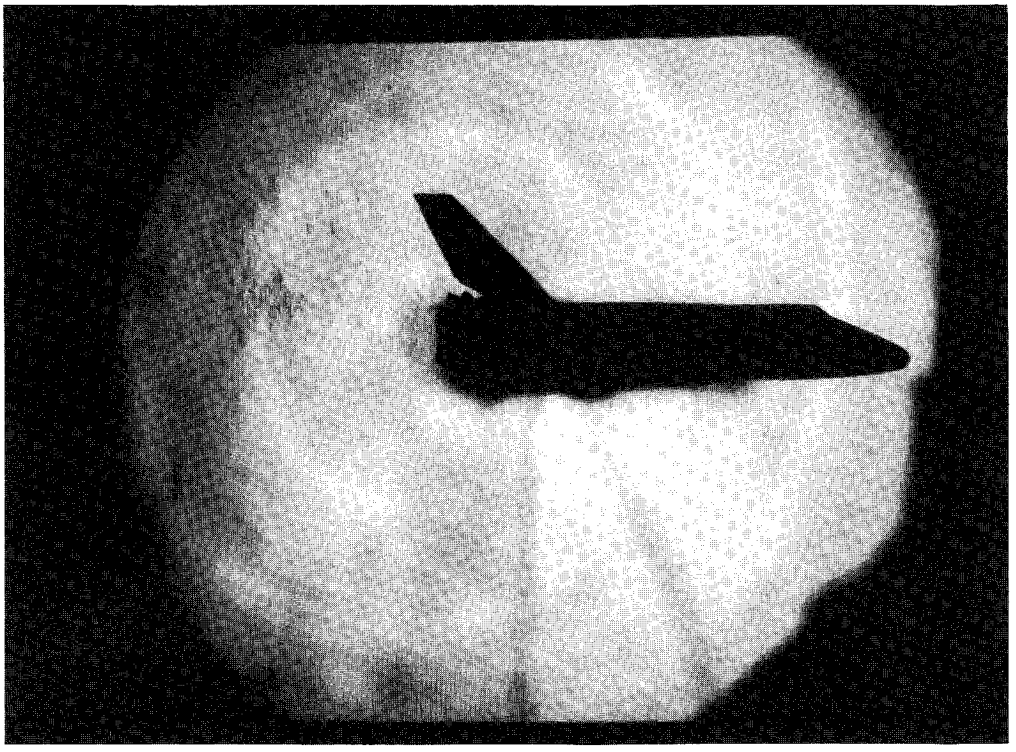

Fig. 5 Modified Space Shuttle model in the 0.3 m TCT; vertical grid, $T_t = 120$ K, $p_t = 5.78$ ata, $M = 0.4$, $R_L = 25.6 \times 10^6$.

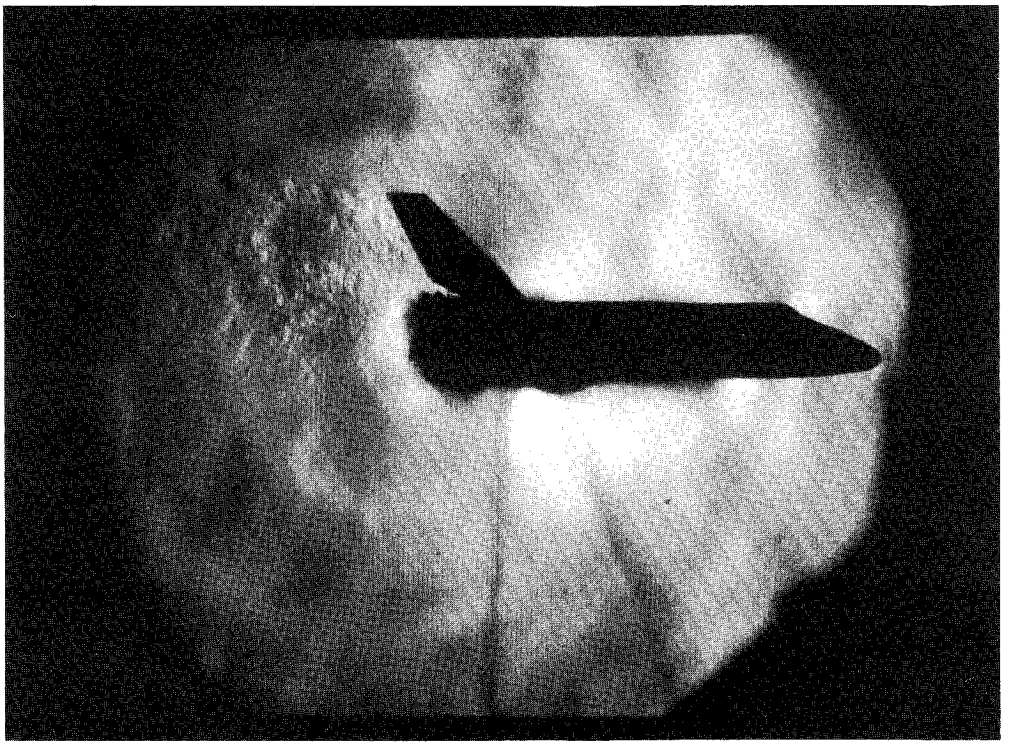

Fig. 6 Modified Space Shuttle model in the 0.3 m TCT; vertical grid, $T_t = 120$ K, $p_t = 5.78$ ata, $M = 0.5$, $R_L = 32.0 \times 10^6$.

board of the 60% semispan station. Although this model's configuration was altered, it was thought that the flow over the body and at the base would be representative of an unaltered blunt configuration. This model was used because of availability and because it has features considered to be relevant to the purpose of the test, i.e., flow visualization. Figure 4 shows details of the base. The vertical tail is deployed in aerobrake mode with a rudder flare of 55 deg. The model included the three main rocket motors' nozzles, as well as two large fairings on the sides representing the housing of the orbital maneuvering system of the vehicle. These details should be noticed, since the base drag may constitute as much as 50% of the total drag during the transonic phase of the unpowered glide toward landing, and because flow visualization can provide relevant information regarding the wake structure and its scales. The base has 15 pressure orifices; the pressure tubes are led outside the model through the wing tips into the plenum where they bend downward and connect to the pressure measurement modules. Even though the bundles of the pressure tubes cross the lower half of the field of view of the focusing schlieren, their image varies between being fuzzy to almost imperceptible because they are

out of the focused image plane. In a regular schlieren system, these tubes would have masked flow features on their optical path.

Because of model structural limitations, most data were taken at $\alpha = 0$ deg; therefore, the discussion will be limited to that angle.

Flow Visualization Results

The experimental setup functioned well all across the temperature, pressure, and Mach number range of the tunnel. The contrast and sensitivity of the system seemed to increase with decreasing temperatures and increasing pressures, both of which increase the flow's density.

Focusing schlieren systems are sensitive to flow density gradients (normal to the strips of the grid), and as such they provide good images of compressible flows. As shown in Fig. 5, this particular setup was sensitive enough to detect wake flows starting at $M = 0.4$, even though the details in these halftone reproductions are degraded with respect to the original black-and-white pictures.

At $M = 0.5$ (see Fig. 6), the wake details appear clearly visible, i.e., the vortices shed by the rudder aerobrake, the orbital maneuvering system, and the two lower main rocket engines' nozzles and those vortices shed by the lower side of the base (showing as a row of pair vortices), altogether four distinct regions. Particularly inter-

Fig. 7 Modified Space Shuttle model in the 0.3 m TCT; vertical grid, $T_t = 120$ K, $p_t = 2.04$ ata, $M = 0.85$, $R_L = 15.6 \times 10^6$.

Fig. 8 Modified Space Shuttle model in the 0.3 m TCT; vertical grid, $T_t = 120$ K, $p_t = 5.78$ ata, $M = 0.85$, $R_L = 44.3 \times 10^6$.

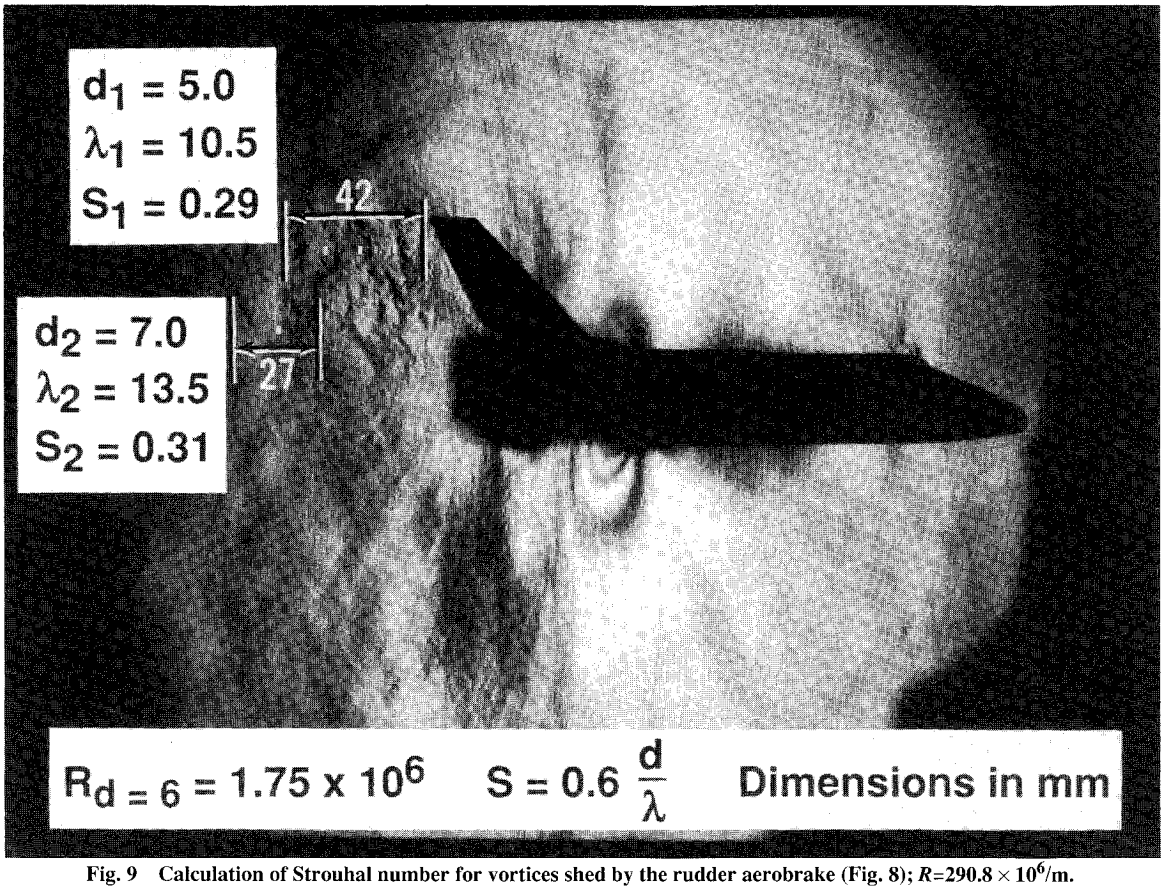

Fig. 9 Calculation of Strouhal number for vortices shed by the rudder aerobrake (Fig. 8); R=290.8 $\times$ 10^6/m.

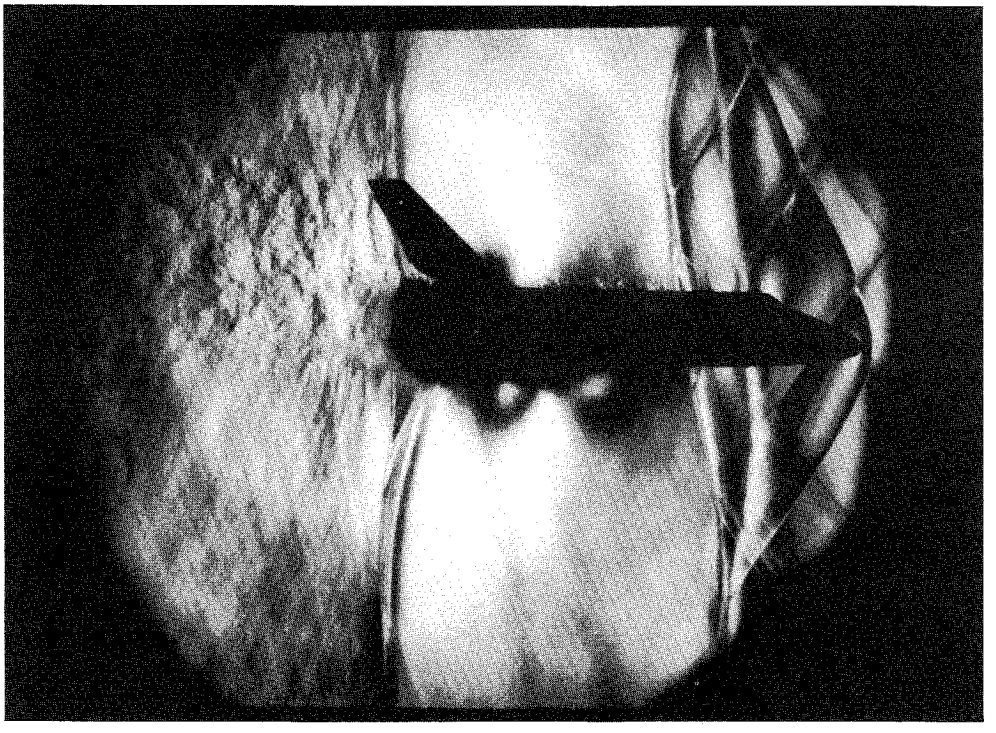

Fig. 10 Modified Space Shuttle model in the 0.3 m TCT; vertical grid, T_T = 140 K, p_t = 3.20 ata, M=1.2, R_L = 21.7 $\times$ 10^6.

esting is the stretching of the vortices shed by the rudder's aerobrake, resulting from viscous entrainment of the freestream. Thus, the top end of these vortices is entrained at a higher speed than their bottom end, and the farther downstream these vortices travel, the more slanted they become.

Figures 7 and 8 were taken at M = 0.85, at 2.04 ata (30 psia) and 5.78 ata (85 psia), respectively, thus increasing the Reynolds number by a factor of approximately 3. At this Mach number, the wind tunnel choked at 85% of the body length, the shock wave being visible at that location. In the fourth quadrant of Fig. 7 (downstream of the shock wave and underneath the wake), the flow displays a fine mesh texture caused by the boundary-layer noise generated in the wind-tunnel diffuser that cannot propagate further upstream being blocked by the choking shock wave. In the same figure, just ahead of the choking shock wave and underneath the model, there is a dark ring, which appears in other pictures as well. Presumably, this is a photoelastic effect of the windows' stress resulting from the aerodynamic forces of the model transmitted

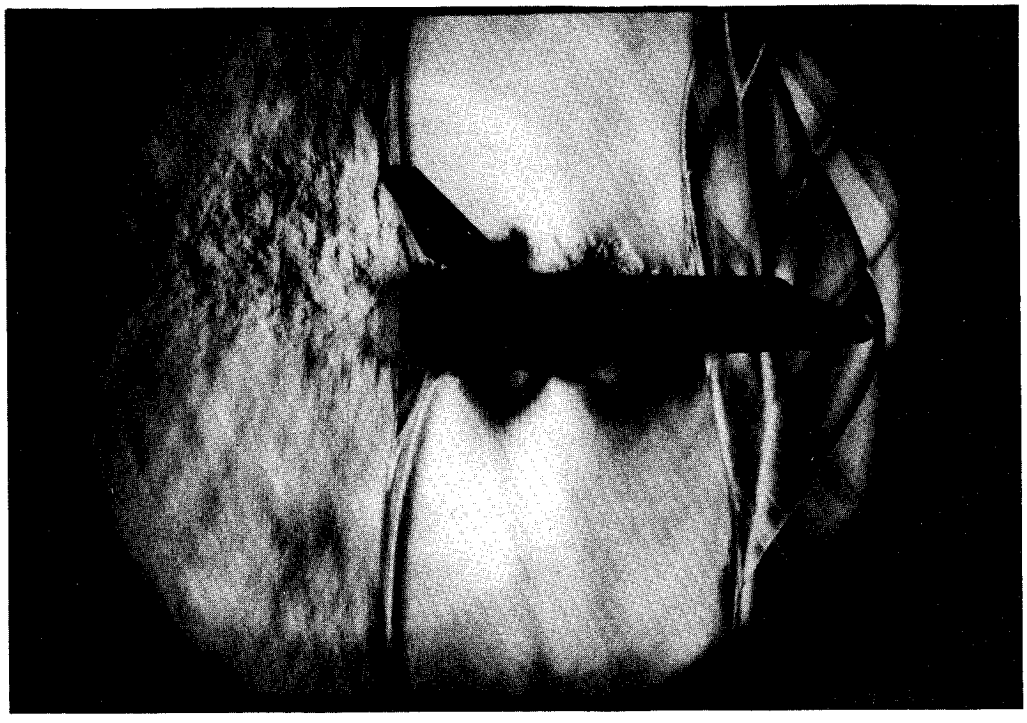

Fig. 11 Modified Space Shuttle model in the 0.3 m TCT. Same conditions as in Fig. 10. Notice boundary-layer separation on top of the body due to pitch oscillations.

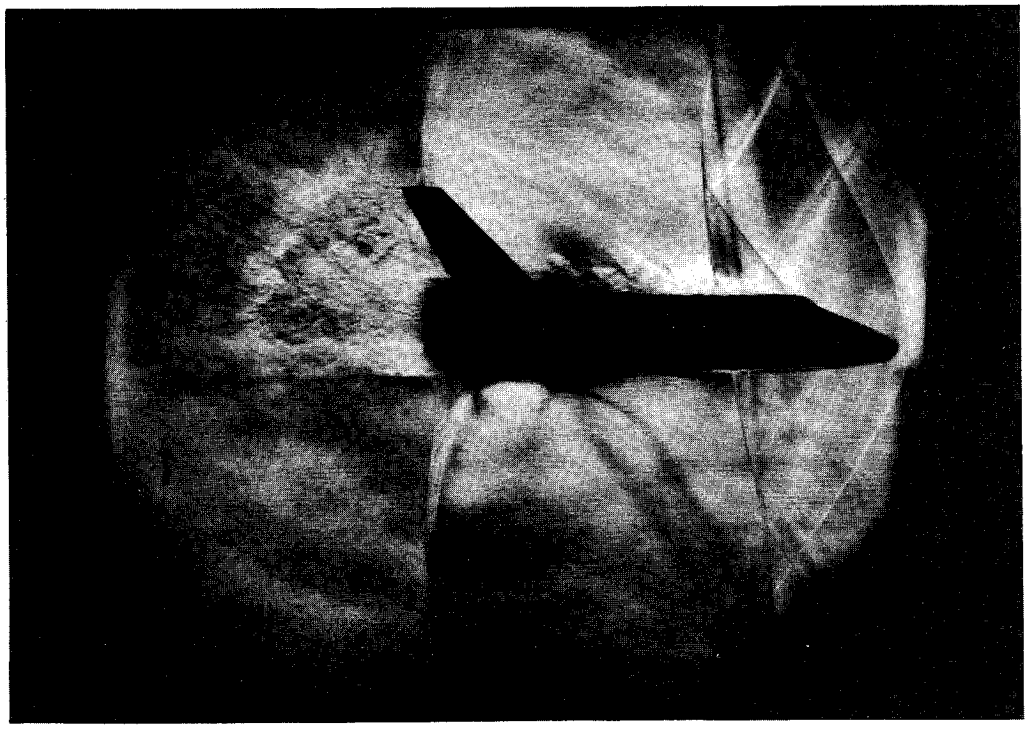

Fig. 12 Modified Space Shuttle model in the 0.3 m TCT. Horizontal grid. Same conditions as in Fig. 10. Notice vortical flow in separated boundary layer atop the model.

through its wing tips. This stress causes the light to deflect at angles exceeding the dynamic range of the cutoff grid (i.e., deflecting more than one pair of strips). In Fig. 8, this effect is enhanced, and the number of rings increases under the higher stress, which is caused by a higher aerodynamic load on the model resulting from the increased dynamic pressure.

An interesting Reynolds number effect can be observed by comparing the shock waves atop the cockpit, in Figs. 7 and 8. The shock wave in Fig. 7 is downstream of the turn and normal. By comparison, the shock in Fig. 8 shifts upstream, occurs just at the turn atop the cockpit, and resembles a λ shock. This may be the result of the boundary-layer relaminarization caused by the flow expansion at the turn.

Of particular interest is the verification as to whether flow features showing in these images can be quantitatively related to similar results reported elsewhere. Since most of the attention is on the wake, the Strouhal number of its vortices comes as a natural choice. Figure 9 is a repetition of Fig. 8, where some of these vortices have been identified. The wavelength of the vortices was deduced from direct measurement on the figure and scaling relative to the model body length, and the dimensions of the local opening of the rudder aerobrake are known, as shown in Fig. 4. Down-

stream from the top of the aerobrake, there are four identifiable vortices, whereas downstream from its bottom there are two. The opening of the aerobrake is $d = 5$ mm for the top location and $d = 7$ mm close to its bottom. The flow parameters were assumed to correspond to the nominal test conditions. Actually, this is an underestimate, since the measurement region is immediately downstream of the normal shock wave that chokes the tunnel, and thus the local air velocity is probably closer to $M = 1$, and the density, static temperature, and viscosity are higher. The unstructured pattern of the vortices and a mean Strouhal number of 0.30 for a mean Reynolds number of 1.75×10^6 based on a mean aerobrake opening of 6 mm is in good agreement with data reported from other investigations.[5] Also notice that the larger aerobrake opening produced a higher Strouhal number and (independently) a higher Reynolds number, which agrees as well with the known trend of this relationship. The wavelength determination is on the upper limit by 1 mm for condition "1" and by 0.5 mm for condition "2" (i.e., the wavelengths may actually be shorter than indicated in Fig. 9), which brings the resulting Strouhal number even closer to the values of Ref. 5.

Figure 10 illustrates the flowfield produced by a failed attempt to start the wind tunnel supersonically for $M = 1.2$ by diverging the adaptive walls starting from a minimum (throat) at the entry to the test section. The interaction between the supersonic flow and the body produces a bow shock, which interacts with shock waves from the walls, mutually bending each other and compressing the flow. The shock interaction region ends with a recovery shock at about 40% of the body length followed by a noise-free section and a second normal shock wave that chokes the tunnel. The wake features are similar to the $M = 0.85$ case presented earlier. At this testing condition, the model oscillated in pitch because of unsteady aerodynamic loading, and the turbulent bursts of the boundary layer, which can be seen just downstream of the recovery shock wave, grow to cause massive boundary-layer separation as illustrated in Fig. 11. The same flow conditions are shown in Fig. 12, this time imaged with a horizontal grid sensitive to vertical pressure gradients. A close examination of the boundary layer atop the body reveals that the separation is actually triggered by the oblique shock atop the cockpit and separates completely only after encountering the large adverse pressure gradient of the recovery shock. The horizontal grid captures the vortical flow in the separated region, part of the attached boundary layer on the lower part of the body, and the various scales of the turbulent structures in the wake.

Conclusions

The first flow visualization with focusing schlieren in a major wind tunnel was performed in the 0.3 m Transonic Cryogenic Tunnel at NASA Langley Research Center. The results indicate the capability of this technique to visualize flows for Mach numbers as low as 0.4. A significant improvement over conventional schlieren systems was the small depth of focus, which limited the visualization to local flow features of the model itself and also blurred completely the large turbulent structures in the plenum. Those parts of the system that had to be placed in the plenum withstood the low temperatures. This installation demonstrates the applicability of such a system in the NTF and other similar cryogenic tunnels. The sensitivity of the system is high enough to capture fine details of wakes, shock waves, and boundary layers, as well as interactions and instabilities of these features. Finally, the low price of the optical components offer the capability to design and adapt focusing schlieren systems to address specific research needs.

Acknowledgments

The first author's research is supported by NASA Langley Research Center, task order NAS 1-18584 #151. The authors express their gratitude to their colleagues Clarence "Buddy" P. Young and Larry C. Rash, for determining allowable test conditions for the model, and Theodore J. Biess, for designing components of the test system.

References

[1]Heppe, R. R., O'Laughlin, B. D., and Celniker, L., "New Aeronautical Facilities—We Need Them Now," *Astronautics and Aeronautics*, Vol. 6, No. 3, 1968, pp. 42–54.

[2]Howe, J. T. (ed.), "Some Fluid Mechanical Problems Related to Subsonic and Supersonic Aircraft," NASA SP-183, 1968.

[3]Goodyer, M. J., and Kilgore, R. A., "High-Reynolds-Number Cryogenic Wind Tunnel," *AIAA Journal*, Vol. 11, No. 5, 1973, pp. 613–619.

[4]Weinstein, L. M., "An Improved Large-Field Focusing Schlieren System," AIAA Paper 91-0567, Jan. 1991; see also "Large-Field High-Brightness Focusing Schlieren System," *AIAA Journal*, Vol. 31, No. 7, 1993, pp. 1250–1255.

[5]Schlichting, H., *Boundary Layer Theory*, 7th ed., McGraw-Hill, New York, 1979, Fig. 2.9, p. 32.